Published in final edited form as:
Magn Reson Med. 2014 March ; 71(3): 1015–1023. doi:10.1002/mrm.24760.

Quantitative MRI Analysis of Menisci Using Biexponential T_2* Fitting with a Variable Echo Time Sequence

Vladimir Juras[1,2,*], **Sebastian Apprich**[1], **Štefan Zbýň**[1], **Lukas Zak**[3], **Xeni Deligianni**[4], **Pavol Szomolanyi**[1], **Oliver Bieri**[4], and **Siegfried Trattnig**[1]

[1]Center of Excellence for High field MR, Department of Radiology, Medical University of Vienna Waehringer Guertel 18–20, Vienna, Austria. [2]Institute of Measurement Science, Department of Imaging Methods, Dubravska cesta 9, Bratislava, Slovakia. [3]Department of Trauma Surgery, Vienna General Hospital, Medical University of Vienna, Vienna, Austria. [4]Division of Radiological Physics, Department of Radiology, University of Basel Hospital, Basel, Switzerland.

Abstract

Purpose—The goal of this study was to differentiate between normal, degenerative meniscus, and meniscal tears using monoexponentially and biexponentially calculated T_2*. Meniscal disease, characterized by an altered collagen fiber matrix, might be detectable in vivo using quantitative T_2* mapping.

Methods—A 3D Cartesian spoiled gradient echo technique was adapted to enable the use of a variable echo time approach in combination with a highly asymmetric readout. T_2* was calculated monoexponentially and biexponentially using three- and five-parametric non-linear fits, respectively.

Results—From a total of 68 evaluated menisci, 48 were normal, 12 were degenerated, and eight had tears. Mean values for the short (T_2*$_s$) and long (T_2*$_l$) T_2* components were as follows: in normal menisci, 0.82 ± 0.38/15.0 ± 5.4 ms, respectively; in degenerated menisci, 1.29 ± 0.53/19.97 ± 5.59 ms, respectively; and, in meniscal tears, 2.05 ± 0.73 and 26.83 ± 7.72 ms, respectively. Biexponentially fitted T_2* demonstrated a greater ability to distinguish normal and degenerated menisci using receiver operating characteristic (ROC) analysis (higher area under curve as well as higher specificity and sensitivity).

Conclusion—This study suggests that biexponential fitting, used for T_2* calculation in the menisci, provides better results compared to monoexponential fitting. Observed changes in T_2* result from the matrix reorganization in degenerative processes in the menisci, which affects the collagen fiber orientation, as well as content.

Keywords

meniscus; tear; degeneration; T_2*; multiple compartment

[*]Correspondence to: Vladimir Juras, Ph.D., Center of Excellence for High field MR, Department of Radiology, Medical University of Vienna Waehringer Guertel 18–20, A-1090 Vienna, Austria. Vladimir.juras@meduniwien.ac.at.

With aging and overloading of the knee joint, the prevalence of meniscal degeneration has increased, which is characterized by the macroscopic changes in meniscal tissue. Such affected menisci become weak and substantially thinner (1). The degeneration of the meniscus is usually accompanied by weakness of the meniscal tissue, which can no longer distribute load sufficiently, and may eventually result in a meniscal tear (2). Grades of meniscal degeneration correlate with grades of articular cartilage degeneration. According to statistics, 85% of osteoarthritis (OA) patients who underwent joint replacement surgery suffer from degenerative menisci (3). Conventional morphologic MR imaging is currently the preferred imaging modality for evaluating the menisci (4). The most commonly used sequences include proton density spin echo or fast spin echo (FSE) with or without fat saturation, T_1-weighted FSE, and gradient echo (GRE) sequences (5). Each of these techniques has a different sensitivity and specificity for the diagnosis of the grade of degeneration in menisci, which are dependent on various factors, such as observer variation or sample size (6–8). Owing to a high degree of tissue organization, the signal decay in menisci is relatively fast. Therefore, on images with longer echo times (TE), menisci usually appear dark. Ultrashort echo time sequences are useful in acquiring the fast-decaying MR signal from meniscal tissue (9,10). Sequences with radial sampling of k-space often suffer from low resolution or pixel blurring due to their sensitivity to gradient imperfections and clock-shift delays (11). The recently introduced, three-dimensional, spoiled gradient echo (SPGR) sequence with a variable echo time scheme (3D vTE Cartesian SPGR, hereafter referred to as vTE) minimizes the abovementioned issues and was shown to be useful for visualizing MSK structures with a short T_1, within short and clinically adequate scan times (12). Collagen fibers in the human meniscus are oriented according to the region: randomly in the superficial network; radially in the lamellar layer; and circularly in the main central layer (13). As the relaxation constants, such as T_1, T_1*, or $T_{1\rho}$, reflect the collagen structure organization in the meniscus, they are regionally dependent (14–16). Quantitative analysis of the meniscus has been suggested in a few recent reports. Rauscher et al. demonstrated that T_1 and $T_{1\rho}$ can be used in the menisci as markers of different stages of OA (15); both T_1 and $T_{1\rho}$ increased in advanced stages of OA. Krishnan et al. studied T_1 in the presence of a gadolinium contrast agent (T_1(Gd)), and found a relationship between T_1(Gd) in the menisci and T_1(Gd) in the cartilage; however, the correlation between T_1(Gd) in the menisci and the grade of meniscal degeneration was minimal (17). Because of the complexity of the collagen matrix in meniscal tissue, it has been assumed that there are bound and free water pools, as well as a relaxation dependence on collagen fiber orientation that results in multicomponent transverse relaxation of magnetization. When calculating T_1 or T_1* using a simple monoexponential fitting, the results may be remarkably underestimated, particularly in the areas with clear bi-component decay. To the best of our knowledge, there is no study that has comprehensively discussed the multiple compartment T_1* mapping of the human menisci in vivo.

Therefore, the aim of this study was to compare the ability of monoexponentially and biexponentially calculated T_2* to differentiate between normal, degenerative meniscus, and meniscal tears. For this purpose, a novel 3D vTE Cartesian SPGR sequence, with sequentially shifted echo times, was used to optimize *T2** sampling in order to offer more accurate quantification of relaxation times. As meniscal disease is characterized by an

altered collagen matrix, these alterations might be detectable in vivo using quantitative T_2* mapping. The regional dependence of monoexponential and biexponential T_2* decay was studied as well.

METHODS

Subjects

The local ethics commission approved this study, and all volunteers and patients gave written, informed consent. Seventeen subjects enrolled in this study (eight males, 34 ± 10 years; and nine females, 36 ± 14 years), all of who underwent a regular check-up that included an MRI examination. Eight patients underwent Matrix Associated Autologous Chondrocyte Transplantation, one of which after a Microfracture procedure, and nine subjects received MRI because of persistent knee pain. The inclusion criteria for all subjects were no contraindications to MR imaging, such as electronically, magnetically, and mechanically activated implants, insulin pumps, nerve stimulators, pregnancy, claustrophobia, and tattoos. Patients with cartilage repair were included since it is well known that full thickness cartilage defects, particularly in the weight-bearing zone, is a risk factor for the development of meniscal lesions (18,19).

MR Imaging

All MRI examinations were performed on a 3T MR system (Tim Trio, Siemens Healthcare, Erlangen, Germany) with an eight-channel knee coil (In vivo, Gainesville, FL). A custom 3D Cartesian SPGR technique was adapted to enable the use of a vTE approach in combination with an asymmetric readout (12). This sequence enables the use of the minimal effective echo time below 1 ms that is necessary for multicomponent T_1* analysis. In addition, the sequence was adapted with sequentially shifted echo times in order to achieve better sampling of the signal decay (20).

The vTE sequence was applied with 10 echoes: TE = [0.75, 3.51, 5.87, 8.23, 10.6, 12.96, 15.33, 17.69, 20.06, and 22.42] ms, and the rest of the parameters were as follows: flip angle 13 degrees; repetition time (TR) 29 ms; and one signal average. The bandwidth was 320 Hz/pixel; 144 sections; with a total acquisition time of 12 min and 16 s. The field of view was 120 × 180 mm, with a consecutive in-plane resolution of 0.47 × 1.02 mm; a slice thickness of 0.7 mm; and matrix size was 256 × 176 pixels.

For morphologic examination, a set of three sequences was used: fat-suppressed proton-density-weighted SPACE in the sagittal plane; PD turbo-spin echo in the coronal plane; and T_2-weighted turbo-spin echo in the sagittal plane. The sequence parameters are summarized in Table 1.

Evaluation of Menisci

All menisci segments were graded morphologically into three groups: normal (grade 0); degenerated (grade 1–2); and meniscal tear (grade 3). Grading was done according to the classification scheme proposed by Crues (21–23): grade 0 - normal signal; grade 1 - intrameniscal focus of signal; grade 2 - intrameniscal linear or wedge-shaped signal; and

grade 3 - linear or globular signal extending to an articular surface. An orthopedic surgeon with 5 years of experience (S.A.) rated the menisci.

Image Analysis

Images from the vTE sequence were analyzed using a custom-written script in IDL 6.3 (Interactive Data Language, Research Systems, Inc, Boulder, CO, USA). A monoexponential as well as a biexponential fitting procedure was employed on all MR data sets on a pixel-by-pixel basis. For monoexponential fitting, a three-parametric function was used to fit the signal intensity

$$S_{\mathrm{m}} = A_0 * \ exp\left(-TE/A_1\right) + A_2 \quad (1)$$

where A_0 is the signal intensity at a TE of ~0 ms, A_1 corresponds to the actual $T_2{}^*_{\mathrm{m}}$ (monoexponentially calculated T_2*), and A_2 is the baseline (mostly the noise). The same dataset was also processed biexponentially, using the function

$$S_{\mathrm{b}} = B_0 * \ exp\left(-TE/B_1\right) + B_2 * \ exp\left(-TE/B_3\right) + B_4 \quad (2)$$

where B_1 corresponds to the short component of T_2* ($T_2{}^*_{\mathrm{s}}$), B_3 corresponds to the long component of T_2* ($T_2{}^*_{\mathrm{l}}$), and B_0 and B_2 are the component ratios expressed further as a percentage value of $B_0 + B_2$: F_s $100*B_0/(B_0 + B_2)$ and $F_l = 100*B_2/(B_0 + B_2)$. B_4 is the offset given primarily by noise. During the calculation of T_2*, only those pixels that satisfied the following condition were considered biexponential:

$$4 \times T_{2*\mathrm{s}} < T_{2*\mathrm{l}} \quad (3)$$

Seven maps for each slice were stored for future use, i.e., the monoexponential T_2* maps, the short component of biexponential T_2* maps, the long component of biexponential T_2* maps, and both short and long T_2* component ratios. The map of the coefficient of determination (R^2, goodness of fit) and the binary map based on the biexponential condition (Eq.[3]) (0 = monoexponential decay, 1 = biexponential decay) were saved as well.

On each subject's knee, four different menisci areas were segmented: the anterior and posterior horn of the lateral meniscus, and the anterior and posterior horn of the medial meniscus. Regions of interest were defined on five consecutive slices by an orthopedic surgeon with 10 years of experience (S.A.). Each meniscal part was further subdivided into two regions, a red and a white zone so that 30% of the radial dimension of each horn, from its free edge to its peripheral border, was considered the red zone and 70% the white zone (13,24). An example of the meniscal segmentation is depicted in Figure 1.

Each ROI was represented by a weighted mean value, calculated using an R^2 correction algorithm (25). $T_2{}^*_{\mathrm{s}}$ and $T_2{}^*_{\mathrm{l}}$ were calculated using a mask created from a binary map, and only pixels where the condition $4 \times T_2{}^*_{\mathrm{s}} < T_2{}^*_{\mathrm{l}}$ was satisfied, were included. From each segment, the ratio of monoexponential and biexponential pixel amounts was calculated (further referred to as *M/B*).

Intraobserver and Interobserver Variation

To calculate the interobserver variability, 10 patients were evaluated by three independent raters (S.A., V.J., P.S.). The variation between raters was expressed as a coefficient of variation (CV, %). Intraobserver variability was calculated from three independent evaluations of 10 patients by one rater (V.J) with a delay of one week between the evaluations and expressed as an intraclass correlation (ICC).

Statistical Analysis

All statistical calculations were performed using SPSS 19.0 and the package pROC version 1.5.4 of R (R Core Team, 2012). Descriptive statistics were performed in order to calculate the mean and standard deviation (SD) of age, $T_1{}^*_m$, $T_1{}^*_s$, $T_1{}^*_l$, component ratios, and *M/B* values separately for normal, degenerative, and torn menisci. In order to compare average $T_1{}^*_m$, $T_1{}^*_s$, $T_1{}^*_l$, and *M/B* of different meniscal parts (anterior/posterior, medial/lateral, healthy/degenerated/tear) a hierarchical linear model (HLM) was used in order to consider multiple measures per patient. In addition, ROC analyses were performed to compare healthy with combined degenerated and torn meniscal parts. A p value equal to or below 0.05 was considered to indicate significant results. A binary classification test was performed on the data to obtain the discrimination power using ROC analyses. ROC curves were constructed by plotting the fraction of true positives from the positives (true positive rate) versus the fraction of false-positives from the negatives (false-positive rate), at various threshold settings for each of the parameters ($T_1{}^*_m$, $T_1{}^*_s$, $T_1{}^*_l$, and *M/B*). The area under the curve (AUC) was calculated by using the trapezoidal rule, which was expressed in percentages and graded in five groups: 0.9–1.0 excellent; 0.8–0.9 = good; 0.7–0.8 = fair; 0.6–0.7 = poor; and 0.5–0.6 = failed.

RESULTS

The CV for interobserver variation was found to be 9.1%, on average. For different menisci segments, the CV was 9.5% for the red zone of the anterior horn, 7.9% for the white zone of the anterior horn, 10.8% for the white zone of the posterior horn, and 8.2% for the red zone of the posterior horn, separately, and 8.0% for the whole white zone and 10.16% for the whole red zone. Intraobserver variation was expressed using ICC and found to be 0.9, on average. For different segments, the ICC was 0.847 for the red zone of the anterior horn, 0.945 for the white zone of the anterior horn, 0.925 for the white zone of the posterior horn, and 0.874 for the red zone of the posterior horn, separately, and 0.935 for the whole white zone and 0.861 for the whole red zone.

The mean and SD for the pixel count were as follows: in the anterior horn, 17 ± 4 (red zone); in the white zone, 37 ± 6; and, in the posterior horn, 22 ± 5 (red zone) and 42 ± 10 (white zone).

From a total of 68 evaluated menisci segments, 48 were graded as normal, 12 as degenerated, and eight as torn. Six patients underwent a surgical procedure after the MR examination. One normal meniscus, one degenerated meniscus, and four meniscal tears were confirmed by a surgeon through visual examination to be in agreement with the results of

the MRI evaluation. Examples of T_2* maps for a degenerative meniscus and a meniscal tear are depicted in Figures 2 and 3. The results from descriptive statistics for all relaxation parameters are summarized in Table 2 and in a set of box-plots in Figure 4. When considering the red and white zones of the menisci separately, from 48 cases of normal menisci, the mean and SD of $T_2{}^*_m$ was 7.89 ± 1.25 ms in the white zone, and 10.49 ± 3.26 ms in the red zone. This difference was statistically significant (P = 0.026, 95% CI −4.25 to −0.27). As for the results of biexponential analysis, the difference between the red and white zones was statistically significant only for the *M/B* ratio (P = 0.017, 95% CI 0.55–3.49). The results for different segments of menisci with different grades are summarized in Table 3.

Mean values of $T_2{}^*_s$ and $T_2{}^*_l$ were as follows: in normal menisci 0.82±0.38 ms and 15.0±5.4 ms, respectively; in degenerated menisci 1.29±0.53 ms and 19.97±5.59 ms, respectively; and in meniscal tears 2.05±0.73 ms and 26.83±7.72 ms, respectively. Monoexponential fitting provided the following results: 7.61±2.49 ms, 9.54±2.25 ms, and 14.59±5.24 ms, in normal, degenerative, and meniscal tears, respectively. The t-test showed significant differences between both mono and biexponentially calculated T_2* in various menisci conditions. However, the p-values were much lower for the short and long T_2* components compared to monoexponential T_2* results. The p-values of $T_2{}^*_m$ and the *M/B* ratio were similar. All p-values are summarized in Table 4. When comparing the medial and lateral menisci, no statistical difference was found in either parameter, and, for the anterior versus posterior horns, the only difference in means was found in the *M/B* ratio (Fig. 5).

The ROC analysis showed mostly fair to good diagnostic value for both the short and long components, as well as for the mono-/bi-ratio value. Table 5 lists the summary of areas under curve for individual parameters. Regarding the differences between the AUC of individual parameters, no statistically significant difference was observed: AUC(*M/B*) versus AUC($T_2{}^*_s$) p=0.4192; AUC(*M/B*) versus AUC($T_2{}^*_l$) p=0.8053; and AUC($T_2{}^*_s$) versus AUC($T_2{}^*_m$); p=0.5903.

DISCUSSION

Here, we propose a technique for in vivo, quantitative, bi-component T_1* analysis of the human meniscus based on a 3D vTE Cartesian SPGR sequence with sequentially shifted echo times. The results of this study showed that biexponential analysis of the human meniscus in vivo may better distinguish between normal and degenerative menisci, as well as meniscal tears, compared to uncorrected, monoexponential decay. These differences most likely reflect the compositional alteration of the collagen matrix, which is most pronounced in meniscal tears, but is also present in degenerative menisci.

Three layers have been described in the meniscus by electron microscopy imaging: the superficial layer; the lamellar layer; and the central main layer (26). However, with the current set-up, we were unable to distinguish between these zones. Meniscal tissue tears occur along the circular main course of the collagen fibrils in the majority of meniscus lesions (horizontal tear, longitudinal tear, bucket-handle tear) (26). It is important to distinguish between degenerative and traumatic tears (1). There is a strong relationship

between meniscal damage, degenerative tears, and cartilage loss (27). However, in this study, we did not look at the relationship between cartilage state and meniscus impairment.

Transversal relaxation time (T_2), as well as T_2 that includes magnetic field inhomogeneities (T_2*), are sensitive to the macromolecular content in tissue, especially glycosaminoglycans and collagen fibers, as has been shown in cartilage studies (14,28). Collagen orientation and anisotropy primarily define the absolute values of T_2 in meniscus (29) and cartilage (30). Higher collagen content and the greater organization of the collagen fiber network in menisci result in substantially shorter transversal relaxation times compared to articular hyaline cartilage.

To the best of our knowledge, meniscal degeneration was previously studied using quantitative MR imaging by only a few groups. Williams and colleagues studied monoexponential T_2*, measured by UTE, as a potential marker for degenerative menisci (31). They observed significantly lower T_2* values in asymptomatic volunteers (9.8 ms) than in patients with meniscal degeneration (18.3 ms). T_2* also correlated strongly with the degree of joint pathology. Rauscher and colleagues successfully used T_2 as a marker for detecting early OA stages through meniscal matrix analysis, and also showed that T_2 relaxation times in menisci correlate with the morphologic score of cartilage in OA (15). In the same study, it was shown that T_1 relaxation time in a rotating frame ($T_{1\rho}$) also has the potential to be used as a marker for distinguishing between healthy and degenerated menisci. The differences in T_2 relaxation times between young male and female volunteers were studied by Tsai et al. (32). They found a statistically significant difference in T_2 values between males and females in the red and white zones; the T_2 values were significantly lower in men than in women (mean difference, 1.320 and 0.865 ms; P=0.002 and $P < 0.001$, respectively). They attributed these differences to the sex differences in the occurrence of knee OA.

Recently, an initial attempt to analyze the menisci using a biexponential fitting procedure was performed in an in vitro porcine model (33). In contrast to the current study, high-resolution MR images were used because of the microimaging capabilities (resolution of 0.27 mm per pixel), which enabled visualization of the laminar structure of meniscal tissue. It was postulated that the transfer to in vivo conditions might be limited, to some extent. However, the SPGR-based vTE sequence used in this study allowed the acquisition of images with relatively high resolution (0.47 × 1.02 mm/px), and in reasonable scan times. The selection of TE range is critical for biexponential fitting. Acquired TEs should be, at best, more dense in the first quarter of the fitting curve to allow the fitting algorithm to calculate the short T_2* component precisely enough, and to distinguish T_2*$_s$ from T_2*$_l$.

The CV between observers was quite low in this study (7.5%); this is probably due to the excellent contrast between menisci and surrounding tissues. For the same reason, the intraobserver variation (ICC = 0.92) was also very low. The high reproducibility can be attributed to the SPGR-vTE sequence, which allows subtracting very short TE images (0.75 ms) from those measured with conventional TEs, resulting in an optimal contrast created by short T_2 tissues (34,35).

Compared to conventional radial 3D-UTE sequences, the vTE sequence has the advantage of the intrinsic robustness of Cartesian sampling methods, and allows high-resolution imaging within reasonable scan times (20). This sequence also enables the use of common acceleration methods, such as partial Fourier or parallel imaging techniques. It also allows measurements in off-center conditions or with nonisotropic voxel sizes.

The receiver operating characteristic analysis in this study suggested a relatively high specificity and sensitivity for this method. The area under curve for $T_2{}^*_s$ was similar to that of $T_2{}^*_m$; however, the sensitivity and specificity was higher for $T_2{}^*_s$ compared to $T_2{}^*_m$ (93 and 77% versus 80 and 79%, respectively). Regarding the threshold for distinguishing between normal and degenerative menisci, or tears, neither of the investigated parameters was able to accomplish this. However, when degenerative menisci and meniscal tears were pooled, it was possible to determine the thresholds.

The higher variability of all parameters ($T_2{}^*_m$, $T_2{}^*_l$, $T_2{}^*_m$ and *M/B*) in normal menisci compared to degenerative menisci and meniscal tears can be attributed to the higher number of cases of normal menisci (48) compared to 12 degenerative menisci and eight tears; thus, the likelihood of outliers is much higher. However, all data had a normal distribution.

Our study has several limitations. First, there was a small number of patients and, in addition, the group of patients was not distributed equally. Second, the ‘magic angle effect’ can influence $T_2{}^*$ values due to the minimization of the dipolar interactions of fiber orientation with respect to B_0 (36–38). To minimize the ‘magic angle effect,’ the ROIs in this study were defined through five consecutive slices in the anterior and posterior horn separately. We believe that the menisci segmentation used in this study was sufficient for evaluating meniscal degeneration and meniscal tears without significant influence from the ‘magic angle effect.’

Third, no histologic assessment was performed in order to confirm the MRI findings. The diagnosis relied fully on the evaluation of morphologic MRI. Only six subjects underwent a surgical procedure in which the problematic menisci were visually confirmed. Histologic evaluations would improve the validity of lesion confirmation, but, MRI is already a fully established modality for the diagnosis of meniscal problems (39–41) even with the known limitations, such as the fact that not every intrameniscal signal seen on MRI represents meniscal degeneration. Also, the pathology at the body of the meniscus was not covered in this study.

Some bias may have also been introduced by choosing the biexponential condition to $4 \times T_2{}^*_s < T_2{}^*_l$, which was based on empiric findings. This choice seemed to best fit the mathematical model of biexponential fitting at the noise level observed in this study; however, no thorough simulations were performed to validate this.

Another complication may have been introduced by local B_0 inhomogeneities, which might have affected $T_2{}^*$ estimation. Although several methods for static magnetic field have been developed (42–44), we did not perform B_0 mapping in this study. However, we know from our previous experience with our MR scanner that there are no substantial B_0 fluctuations other than those caused by anisotropy of the tissue.

CONCLUSION

In conclusion, the results of this study suggest that a biexponential analysis of meniscal tissue is more robust than a monoexponential approach. The short component of T_1* better reflects the anisotropy of collagen fibers and the change in degeneration processes that may result in meniscal tear.

ACKNOWLEDGMENTS

The authors thank Claudia Kronnerwetter for help with MRI scanning and Michael Weber for help with statistical analysis.

Grant sponsor: Austrian Science Fund; Grant number: P 25246 B24; Grant sponsor: the Vienna Advanced Imaging Center (VIACLIC), and the Slovak Scientific Grant Agency VEGA; Grant number: 2/0090/11.

REFERENCES

1. Noble J, Hamblen DL. The pathology of the degenerate meniscus lesion. J Bone Joint Surg Br. 1975; 57:180–186. [PubMed: 1173585]
2. Fahmy NRM, Williams EA, Noble J. Meniscal pathology and osteoarthritis of the knee. J Bone Joint Surg Br. 1983; 65:24–28. [PubMed: 6687393]
3. Sun Y, Mauerhan DR, Honeycutt PR, Kneisl JS, Norton JH, Hanley EN Jr, Gruber HE. Analysis of meniscal degeneration and meniscal gene expression. BMC Musculoskelet Disord. 2010; 11:19. [PubMed: 20109188]
4. Fox MG. MR imaging of the meniscus: review, current trends, and clinical implications. Radiol Clin North Am. 2007; 45:1033–1053. [PubMed: 17981182]
5. Helms CA. The meniscus: recent advances in MR imaging of the knee. AJR Am J Roentgenol. 2002; 179:1115–1122. [PubMed: 12388483]
6. Oei EH, Nikken JJ, Verstijnen AC, Ginai AZ, Myriam Hunink MG. MR imaging of the menisci and cruciate ligaments: a systematic review. Radiology. 2003; 226:837–848. [PubMed: 12601211]
7. De Smet AA, Norris MA, Yandow DR, Graf BK, Keene JS. Diagnosis of meniscal tears of the knee with MR imaging: effect of observer variation and sample size on sensitivity and specificity. AJR Am J Roentgenol. 1993; 160:555–559. [PubMed: 8430552]
8. De Smet AA, Tuite MJ. Use of the ‘two-slice-touch’ rule for the MRI diagnosis of meniscal tears. AJR Am J Roentgenol. 2006; 187:911–914. [PubMed: 16985134]
9. Gatehouse PD, Thomas RW, Robson MD, Hamilton G, Herlihy AH, Bydder GM. Magnetic resonance imaging of the knee with ultrashort TE pulse sequences. Magn Reson Imaging. 2004; 22:1061–1067. [PubMed: 15527992]
10. Robson MD, Gatehouse PD, Bydder M, Bydder GM. Magnetic resonance: an introduction to ultrashort TE (UTE) imaging. J Comput Assist Tomogr. 2003; 27:825–846. [PubMed: 14600447]
11. Nielles-Vallespin S, Weber MA, Bock M, Bongers A, Speier P, Combs SE, Wohrle J, Lehmann-Horn F, Essig M, Schad LR. 3D radial projection technique with ultrashort echo times for sodium MRI: clinical applications in human brain and skeletal muscle. Magn Reson Med. 2007; 57:74–81. [PubMed: 17191248]
12. Deligianni X, Bär P, Scheffler K, Trattnig S, Bieri O. High-resolution Fourier-encoded sub-millisecond echo time musculoskeletal imaging at 3 Tesla and 7 Tesla. Magn Reson Med. 2013; 70:1434–1439. [PubMed: 23233430]
13. Fox AJS, Bedi A, Rodeo SA. The basic science of human knee menisci: structure, composition, and function. Sports Health. 2012; 4:340–351. [PubMed: 23016106]
14. Mlynarik V, Szomolanyi P, Toffanin R, Vittur F, Trattnig S. Transverse relaxation mechanisms in articular cartilage. J Magn Reson. 2004; 169:300–307. [PubMed: 15261626]

15. Rauscher I, Stahl R, Cheng J, Li XJ, Huber MB, Luke A, Majumdar S, Link TM. Meniscal measurements of T1(rho) and T2 at MR Imaging in healthy subjects and patients with osteoarthritis. Radiology. 2008; 249:591–600. [PubMed: 18936315]
16. Du JA, Carl M, Diaz E, Takahashi A, Han E, Szeverenyi NM, Chung CB, Bydder GM. Ultrashort TE T(1)rho (UTE T(1)rho) Imaging of the achilles tendon and meniscus. Magn Reson Med. 2010; 64:834–842. [PubMed: 20535810]
17. Krishnan N, Shetty SK, Williams A, Mikulis B, McKenzie C, Burstein D. Delayed gadolinium-enhanced magnetic resonance imaging of the meniscus—an index of meniscal tissue degeneration? Arthritis Rheum. 2007; 56:1507–1511. [PubMed: 17469113]
18. Kuroda R, Ishida K, Matsumoto T, Akisue T, Fujioka H, Mizuno K, Ohgushi H, Wakitani S, Kurosaka M. Treatment of a full-thickness articular cartilage defect in the femoral condyle of an athlete with autologous bone-marrow stromal cells. Osteoarthritis Cartilage. 2007; 15:226–231. [PubMed: 17002893]
19. Widuchowski W, Widuchowski J, Trzaska T. Articular cartilage defects: study of 25,124 knee arthroscopies. Knee. 2007; 14:177–182. [PubMed: 17428666]
20. Deligianni, X.; Bär, P.; Scheffler, K.; Trattnig, S.; Bieri, O. Water selective high resolution imaging of short T2 components of the knee at high and ultra high field strenghts. Proceedings of the 20th Annual Meeting of ISMRM; Melbourne, Australia. 2012. p. 3315
21. Crues JV III, Mink J, Levy TL, Lotysch M, Stoller DW. Meniscal tears of the knee: accuracy of MR imaging. Radiology. 1987; 164:445–448. [PubMed: 3602385]
22. Stoller DW, Martin C, Crues JV III, Kaplan L, Mink JH. Meniscal tears: pathologic correlation with MR imaging. Radiology. 1987; 163:731–735. [PubMed: 3575724]
23. Dillon EH, Pope CF, Jokl P, Lynch K. The clinical significance of stage 2 meniscal abnormalities on magnetic resonance knee images. Magn Reson Imaging. 1990; 8:411–415. [PubMed: 2392029]
24. Hauger O, Frank LR, Boutin RD, Lektrakul N, Chung CB, Haghighi P, Resnick D. Characterization of the ‘red zone’ of knee meniscus: MR imaging and histologic correlation. Radiology. 2000; 217:193–200. [PubMed: 11012444]
25. Juras V, Zbyn S, Szomolanyi P, Trattnig S. Regression error estimation significantly improves the region-of-interest statistics of noisy MR images. Med Phys. 2010; 37:2813–2821. [PubMed: 20632592]
26. Petersen W, Tillmann B. Collagenous fibril texture of the human knee joint menisci. Anat Embryol. 1998; 197:317–324. [PubMed: 9565324]
27. Hunter DJ, Zhang YQ, Niu JB, Tu X, Amin S, Clancy M, Guermazi A, Grigorian M, Gale D, Felson DT. The association of meniscal pathologic changes with cartilage loss in symptomatic knee osteoarthritis. Arthritis Rheum. 2006; 54:795–801. [PubMed: 16508930]
28. Fragonas E, Mlynarik V, Jellus V, Micali F, Piras A, Toffanin R, Rizzo R, Vittur F. Correlation between biochemical composition and magnetic resonance appearance of articular cartilage. Osteoarthritis Cartilage. 1998; 6:24–32. [PubMed: 9616436]
29. Henkelman RM, Stanisz GJ, Kim JK, Bronskill MJ. Anisotropy of NMR properties of tissues. Magn Reson Med. 1994; 32:592–601. [PubMed: 7808260]
30. Xia Y, Moody JB, Burton-Wurster N, Lust G. Quantitative in situ correlation between microscopic MRI and polarized light microscopy studies of articular cartilage. Osteoarthritis Cartilage. 2001; 9:393–406. [PubMed: 11467887]
31. Williams A, Qian Y, Golla S, Chu CR. UTE-T2 * mapping detects sub-clinical meniscus injury after anterior cruciate ligament tear. Osteoarthritis Cartilage. 2012; 20:486–494. [PubMed: 22306000]
32. Tsai PH, Chou MC, Lee HS, Lee CH, Chung HW, Chang YC, Huang GS. MR T2 values of the knee menisci in the healthy young population: zonal and sex differences. Osteoarthritis Cartilage. 2009; 17:988–994. [PubMed: 19332176]
33. Kirsch, S.; Kreinest, M.; Reisig, G.; Schad, LR. In vitro mapping of 1H ultrashort T2 and T2* of porcine menisci: analysis of the signal decay reveals collagenous fibril texture. Proceedings of the 20th Annual Meeting of ISMRM; Melbourne, Australia. 2012. p. 275
34. Bae WC, Dwek JR, Znamirowski R, Statum SM, Hermida JC, D’Lima DD, Sah RL, Du J, Chung CB. Ultrashort echo time MR imaging of osteochondral junction of the knee at 3 T: identification

of anatomic structures contributing to signal intensity. Radiology. 2010; 254:837–845. [PubMed: 20177096]

35. Robson MD, Gatehouse PD, So PW, Bell JD, Bydder GM. Contrast enhancement of short T2 tissues using ultrashort TE (UTE) pulse sequences. Clin Radiol. 2004; 59:720–726. [PubMed: 15262547]
36. Erickson SJ, Prost RW, Timins ME. The 'magic angle' effect: background physics and clinical relevance. Radiology. 1993; 188:23–25. [PubMed: 7685531]
37. Mosher TJ, Smith H, Dardzinski BJ, Schmithorst VJ, Smith MB. MR imaging and T2 mapping of femoral cartilage: in vivo determination of the magic angle effect. AJR Am J Roentgenol. 2001; 177:665–669. [PubMed: 11517068]
38. Xia Y. Magic-angle effect in magnetic resonance imaging of articular cartilage: a review. Invest Radiol. 2000; 35:602–621. [PubMed: 11041155]
39. Chen MC, Shih TTF, Jiang CC, Su CT, Huang KM. MRI of meniscus and cruciate ligament tears correlated with arthroscopy. J Formos Med Assoc. 1995; 94:605–611. [PubMed: 8527960]
40. De Smet AA, Mukherjee R. Clinical, MRI, and arthroscopic findings associated with failure to diagnose a lateral meniscal tear on knee MRI. AJR Am J Roentgenol. 2008; 190:22–26. [PubMed: 18094289]
41. Ryzewicz M, Peterson B, Siparsky PN, Bartz RL. The diagnosis of meniscus tears—the role of MRI and clinical examination. Clin Orthop Relat Res. 2007:123–133. [PubMed: 17279041]
42. Andris P, Frollo I. Optimized measurement of magnetic field maps using nuclear magnetic resonance (NMR). Meas Sci Technol. 2011; 22:045501.
43. Hornak JP, Szumowski J, Bryant RG. Magnetic-field mapping. Magn Reson Med. 1988; 6:158–163. [PubMed: 3367773]
44. Gruetter R, Tkac I. Field mapping without reference scan using asymmetric echo-planar techniques. Magn Reson Med. 2000; 43:319–323. [PubMed: 10680699]

Europe PMC Funders Author Manuscripts

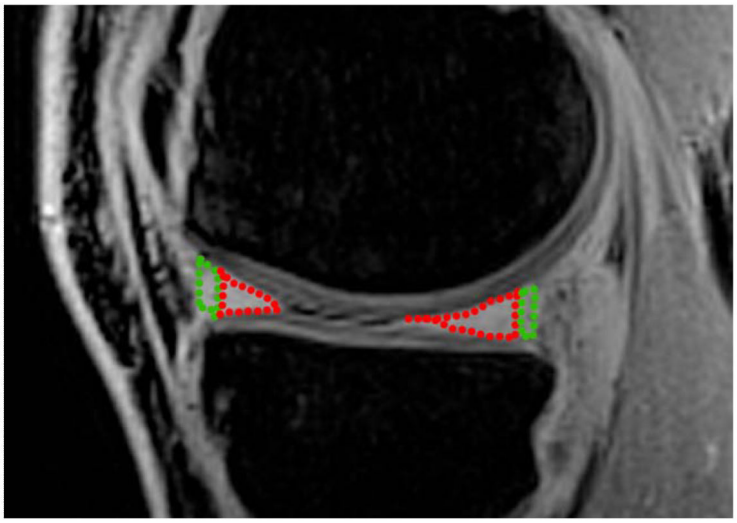

FIG. 1. An example of meniscus segmentation on the difference vTE image that shows the anterior and posterior horn of the lateral meniscus divided additionally into the red zone (green dotted line) and the white zone (red dotted line).

Europe PMC Funders Author Manuscripts

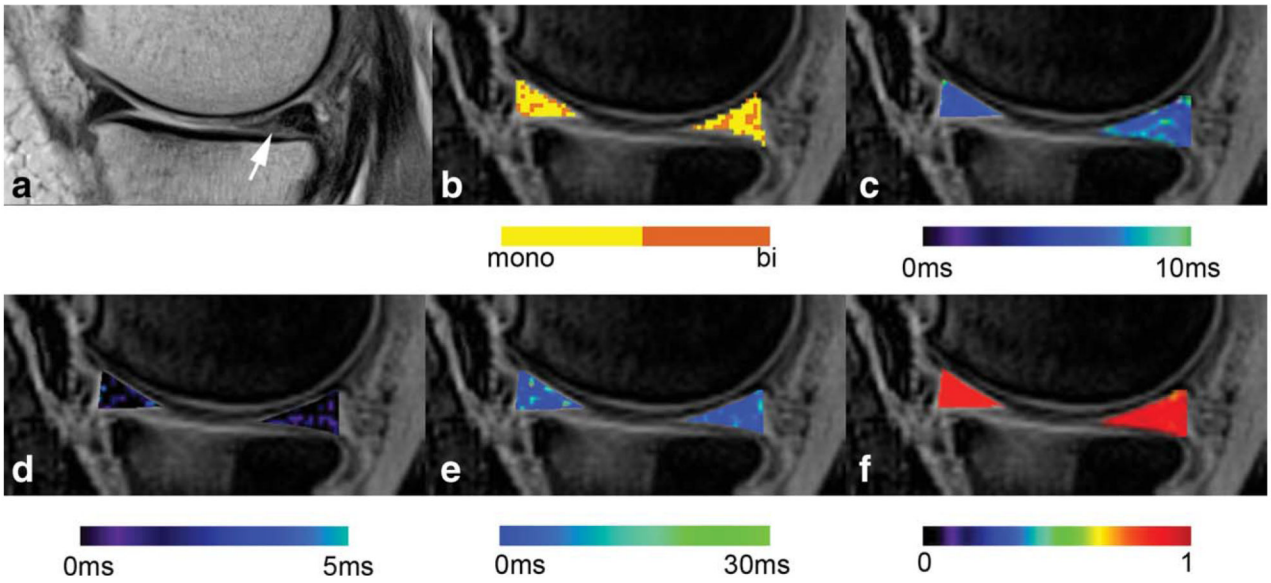

FIG. 2. An example of the map evaluation of a 68-year-old patient with meniscus degeneration (arrow), diagnosed in the posterior horn of the medial meniscus.

a: The morphologic image was acquired with a T_2-weighted turbo-spin echo sequence; (**b**) the binary map of the pixels with biexponential (orange colored) and monoexponential (yellow colored) fit; (**c**) the conventional monoexponential T_2* map; (**d**) the map of the short component T_2* calculated biexponentially; (**e**) the map of the long component T_2* calculated biexponentially; (**f**) the map of the coefficient of variation ($\mathbf{R}^2$) related to the precision of fit. Note that all maps are overlaid on the morphologic image and pseudo-color-coded with the corresponding color bar below each image.

Europe PMC Funders Author Manuscripts

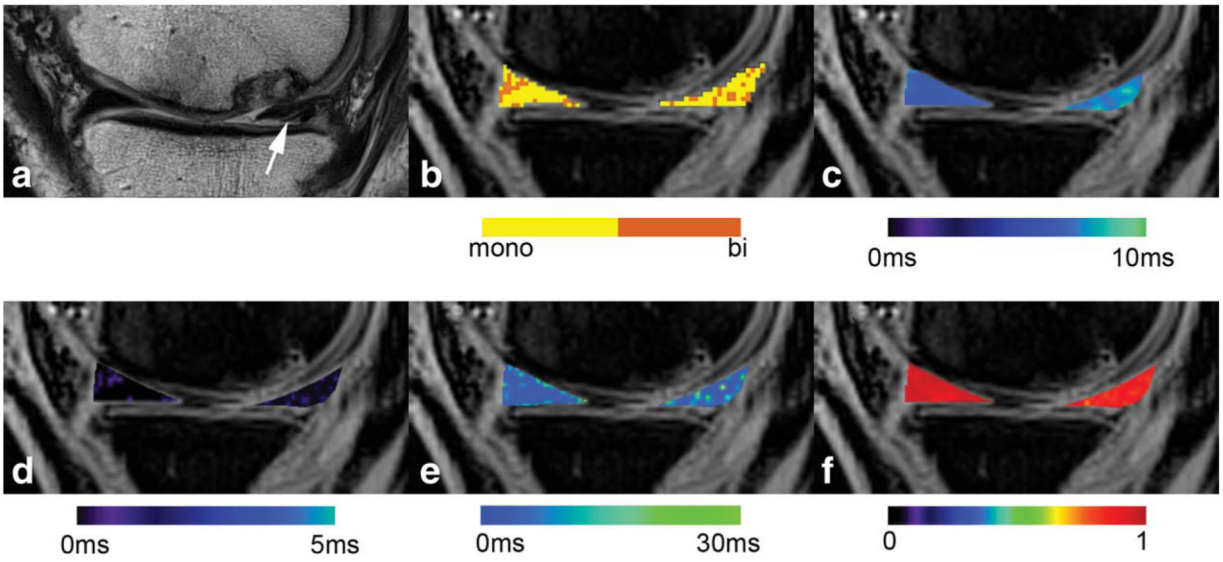

FIG. 3. An example of the map evaluation of a 45-year-old patient with a meniscal tear (arrow), diagnosed in the posterior horn of the medial meniscus.

a: The morphologic image was acquired with a T_2-weighted turbo-spin echo sequence; (**b**) the binary map of the pixels with biexponential (orange colored) and monoexponential (yellow colored) fit; (**c**) the conventional monoexponential T_2* map; (**d**) the map of the short component T_2* calculated biexponentially; (**e**) the map of the long component T_2* calculated biexponentially; (**f**) the map of the coefficient of variation (R^2) related to the precision of fit. Note that all maps are overlaid on the morphologic image and pseudo-color-coded with the corresponding color bar below each image.

Europe PMC Funders Author Manuscripts

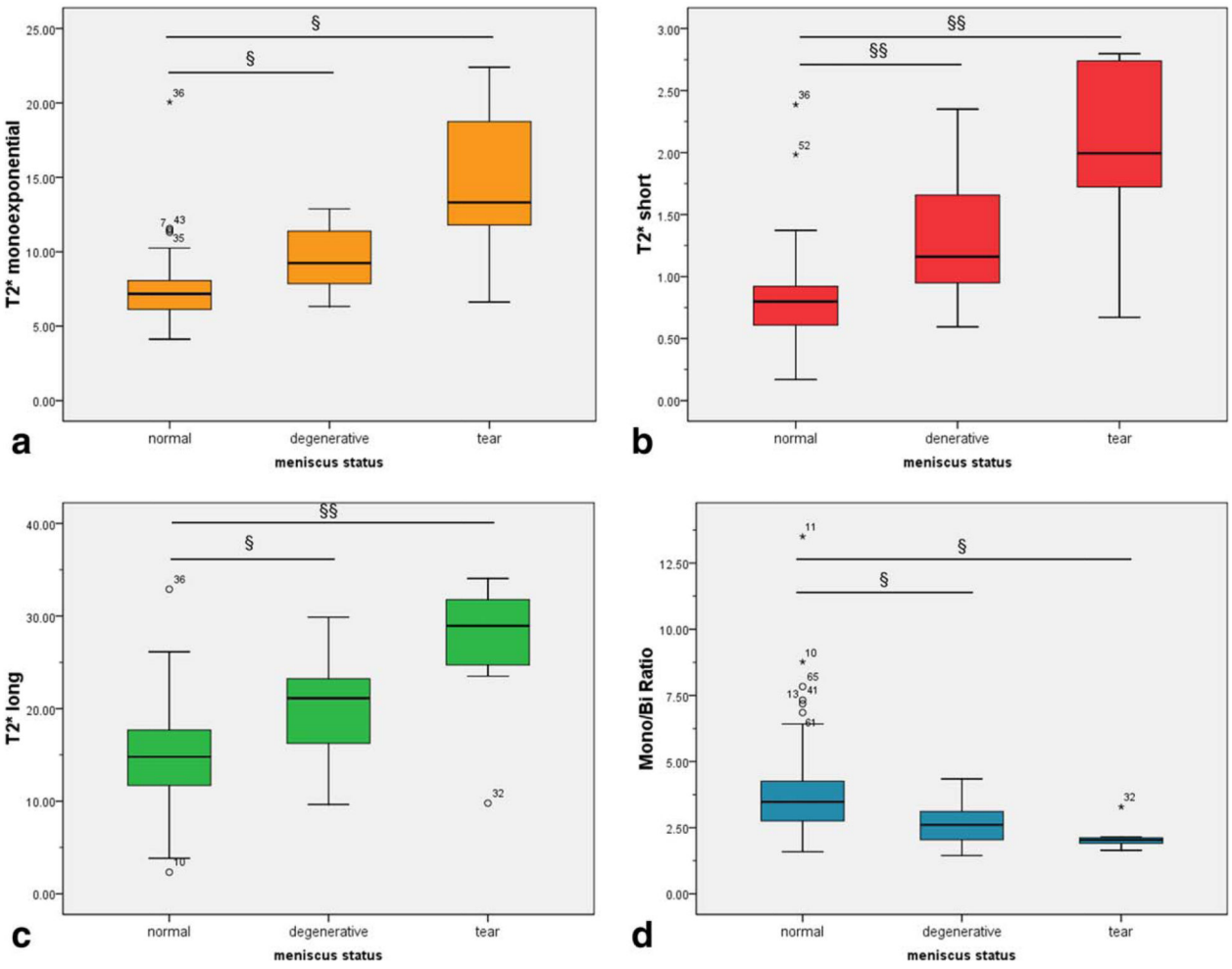

FIG. 4. The box-plot interpretation of monoexponential T_2* (a), short component of T_2* (b), long component of T_2* (c), and the ratio between the pixel with monoexponential and biexponential characteristic (d) values.

Symbols § and §§ indicate statistical significance ($P < 0.05$ and $P < 0.001$, respectively).

Europe PMC Funders Author Manuscripts

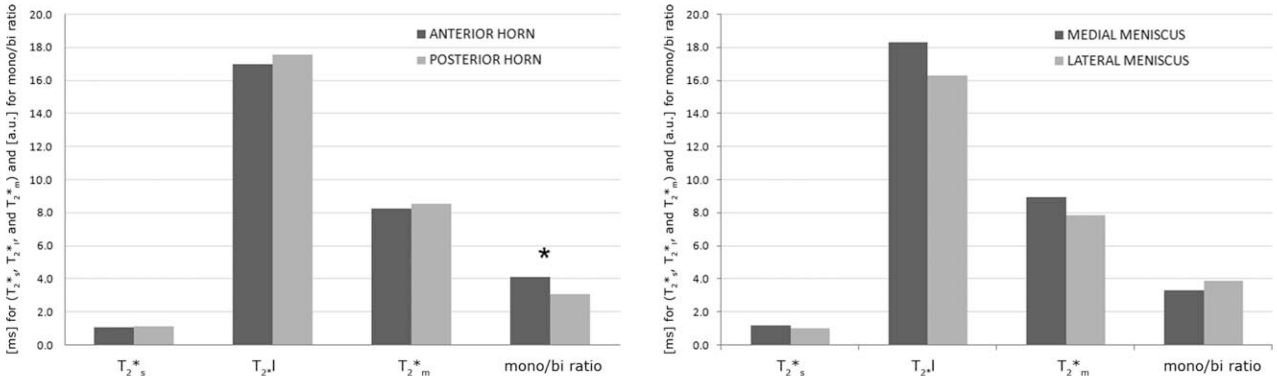

FIG. 5. The difference between the T_2*$_s$, T_2*$_l$, T_2*$_m$, and *M/B* ratio in the medial versus lateral menisci and the anterior versus posterior horns in all subjects.

The asterisk represents statistical significance ($P < 0.05$).

Europe PMC Funders Author Manuscripts

Europe PMC Funders Author Manuscripts

Table 1
The Parameters for the Sequences Used for Morphologic Evaluation of the Knees

	PD-SPACE	PD-TSE	T_2-TSE
Orientation	Sagittal	Coronal	Sagittal
TE (ms)	21	27	94
TR (ms)	1100	4250	2850
FOV read (mm)	175	150	150
FOV phase (%)	93.8	100	100
PAT mode	GRAPPA	GRAPPA	GRAPPA
Acceleration factor	2	2	2
Averages	1	1	3
Slices	160	36	13
Slice thickness (mm)	0.7	3.0	3.0
Bandwidth (Hz/px)	381	150	178
Base resolution	320	384	384

PD-SPACE, fat-suppressed proton-density-weighted SPACE in the sagittal plane; PD-TSE, proton-density turbo-spin echo in the coronal plane; T_2-TSE, T_2-weighted turbo-spin echo in the axial plane; TE, echo time; TR, repetition time; FOV, field of view; PAT, parallel acquisition technique; GRAPPA, parallel acquisition techniques generalized autocalibrating partially parallel acquisitions.

Table 2

Summary of Mean Values for Monoexponential T_2*$_m$, the Short and Long Components of T_2* Calculated Biexponentially, T_2*$_s$, and T_2*$_l$, Respectively, and the Ratio Between Monoexponential and Biexponential Pixel Count (*M/B* ratio) Calculated from Both Horns of the Lateral and Medial Menisci

	Status	Number of cases	Mean value	Standard deviation	R^2
T_2*$_m$ (ms)	Normal	48	7.61	2.49	0.985
	Degenerated	12	9.54	2.25	0.981
	Tear	8	14.59	5.24	0.974
	Anterior horn	34	8.22	2.98	0.986
	Posterior horn	34	8.49	3.56	0.987
T_2*$_s$ (ms)	Normal	48	0.82	0.38	0.991
	Degenerated	12	1.29	0.53	0.986
	Tear	8	2.05	0.73	0.979
	Anterior horn	34	1.03	0.58	0.997
	Posterior horn	34	1.07	0.63	0.967
T_2*$_l$ (ms)	Normal	48	15.0	5.4	0.991
	Degenerated	12	19.97	5.59	0.986
	Tear	8	26.83	7.72	0.979
	Anterior horn	34	16.98	6.90	0.997
	Posterior horn	34	17.55	7.00	0.967
T_2*$_s$ component ratio (%)	Normal	48	64.76	6.08	–
	Degenerated	12	64.95	6.41	–
	Tear	8	70.87	5.84	–
	Anterior horn	34	66.48	6.63	–
	Posterior horn	34	64.54	5.98	–
T_2*$_l$ component ratio (%)	Normal	48	35.24	5.73	–
	Degenerated	12	35.05	6.20	–
	Tear	8	29.13	7.41	–
	Anterior horn	34	33.52	7.25	–
	Posterior horn	34	35.46	8.61	–
M/B (a.u.)	Normal	48	3.88	1.73	–
	Degenerated	12	2.7	0.88	–
	Tear	8	2.13	0.49	–
	Anterior horn	34	4.06	2.41	–
	Posterior horn	34	3.05	1.30	–

R^2 indicates the coefficient of determination.

Table 3

The Differences in the $T_2^*_m$, $T_2^*_s$, $T_2^*_l$, and *M/B* Ratio Between Different Menisci States in the Red and White Zones

	Status	Number of cases	Zone	Mean value	Standard deviation
$T_2^*_m$	Normal	48	Red	7.89	1.25
			White	10.49	3.26
	Degenerated	12	Red	7.12	2.80
			White	9.91	1.89
	Tear	8	Red	14.15	6.24
			White	15.89	5.44
$T_2^*_s$	Normal	48	Red	0.71	0.29
			White	0.82	0.36
	Degenerated	12	Red	1.35	0.51
			White	1.22	0.38
	Tear	8	Red	2.29	0.43
			White	2.12	0.28
$T_2^*_l$	Normal	48	Red	16.81	6.41
			White	14.85	3.77
	Degenerated	12	Red	18.22	5.89
			White	19.78	8.40
	Tear	8	Red	27.38	10.14
			White	24.88	8.97
M/B	Normal	48	Red	3.51	1.28
			White	5.53	2.51
	Degenerated	12	Red	2.40	1.01
			White	4.74	0.87
	Tear	8	Red	1.44	0.74
			White	3.52	1.21

Europe PMC Funders Author Manuscripts

Table 4

The Difference in Monoexponentially and Biexponentially Calculated T_2* Between Normal and Degenerated Menisci and Meniscal Tears

Interactions	T_2*s	T_2*l	*M/B*	T^*_m
MED/LAT	0.704	0.547	0.274	0.626
ANT/POS	0.661	0.563	0.461	0.256
STATUS	0.000[a]	0.000[a]	0.000[a]	0.000[a]
MED/LAT × ANT/POS	0.057	0.857	0.493	0.556
MED/LAT × STATUS	0.001[a]	0.509	0.272	0.225
ANT/POS × STATUS	0.898	0.404	0.014[a]	0.097
MED/LAT × ANT/POS × STATUS	0.150	0.433	0.744	0.749

MED, medial meniscus; LAT, lateral meniscus; ANT, anterior horn of meniscus; POS, posterior horn of meniscus; STATUS, normal, degenerative, or tear.

[a] Statistical significance.

Table 5

The ROC Analysis of Four Different Parameters for the Differentiation Between Normal Menisci and Menisci with Lesions (Degeneration and Tears Combined)

Normal versus menisci with lesion							
	Area under curve	Standard error[a]	Asymptotic 95% confidence interval		Specificity (%)	Sensitivity (%)	Threshold
			Lower bound	Upper bound			
$T_2^*{}_m$	0.824	0.060	0.716	0.952	80	79	7.86 ms
$T_2^*{}_s$	0.834	0.067	0.672	0.933	93	77	0.93 ms
$T_2^*{}_l$	0.802	0.059	0.707	0.941	65	93	22.54 ms
M/B	0.792	0.059	0.676	0.908	65	68	2.96

[a]Under the nonparametric assumption.